*J. Fluid Mech.* (2007), *vol.* 576, *pp.* 349–376.  
doi:10.1017/S0022112006004307 Printed in the United Kingdom

# The role of forcing in the local stability of stationary long waves. Part 1. Linear dynamics

DANIEL HODYSS[1]† AND TERRENCE R. NATHAN[2]

[1]Rosenstiel School of Marine and Atmospheric Science, University of Miami, Miami, Florida, USA

[2]Atmospheric Science Program, Department of Land, Air, and Water Resources, University of California Davis, Davis, California, USA

(Received 29 November 2005 and in revised form 10 October 2006)

The local linear stability of forced, stationary long waves produced by topography or potential vorticity (PV) sources is examined using a quasi-geostrophic barotropic model. A multiple scale analysis yields coupled equations for the background stationary wave and low-frequency (LF) disturbance field. Forcing structures for which the LF dynamics are Hamiltonian are shown to yield conservation laws that provide necessary conditions for instability and a constraint on the LF structures that can develop. Explicit knowledge of the forcings that produce the stationary waves is shown to be crucial to predicting a unique LF field. Various topographies or external PV sources can be chosen to produce stationary waves that differ by asymptotically small amounts, yet the LF instabilities that develop can have fundamentally different structures and growth rates. If the stationary wave field is forced solely by topography, LF oscillatory modes always emerge. In contrast, if the stationary wave field is forced solely by PV, two LF structures are possible: oscillatory modes or non-oscillatory envelope modes. The development of the envelope modes within the context of a linear LF theory is novel.

An analysis of the complex WKB branch points, which yields an analytical expression for the leading-order eigenfrequency, shows that the streamwise distribution of absolute instability and convective growth is central to understanding and predicting the types of LF structures that develop on the forced stationary wave. The location of the absolute instability region with respect to the stationary wave determines whether oscillatory modes or envelope modes develop. In the absence of absolute instability, eastward propagating wavetrains generated in the far field can amplify via local convective growth in the stationary wave region. If the stationary wave region is streamwise symmetric (asymmetric), the local convective growth results in a local change in wave energy that is transient (permanent).

## 1. Introduction

Observations of atmospheric low-frequency (LF) variability over the Northern Hemisphere (NH) show distinct structures in different geographical locations (Kushnir & Wallace 1989). These structures manifest as slowly modulated wavetrains over the continents and zonally elongated features over the oceans. We hypothesize

† Present address: Naval Research Laboratory, 7 Grace Hopper Avenue, Monterey, CA 93943-5502, USA. danhodyss@yahoo.com

that these distinct regional structures can be attributed, in part, to the specific way in which the low-pass filtered flow is externally forced.

In the NH, the external forcing is primarily due to mechanical forcing by the continental landmasses and thermal forcing due to longitudinal variations in diabatic heating. The importance of these forcings to the time-mean flow has been recognized since Charney & Eliassen's (1949) seminal work. Although published more than fifty years ago, their words are equally apt today: 'It has for some time been recognized that the quasi-stationary perturbations of the atmosphere are caused by geographically fixed perturbing forces, but the exact nature of these forces has not been well understood.' The relevance of Charney & Eliassen's words today revolves around several related and unresolved issues. One such issue concerns the net time-mean diabatic heating, which depends on contributions from land–sea heating contrasts, variations in sea-surface temperatures, and longitudinal variations in latent heating, all of which can be influenced by and interact with topography (e.g. Held, Ting & Wang 2002). Another issue concerns the time-mean flow, which contains contributions not only from topography and longitudinal variations in diabatic heating, but also from the low-frequency field itself, which may originate either from resonant excitation due to remote forcing (e.g. Li & Nathan 1997 and references therein) or from the local instability of the forced time-mean flow (e.g. Simmons, Wallace & Branstater 1983).

The latter issue forms the basis of this study. In particular, we consider local linear instability as a mechanism for spawning LF disturbances. In contrast to most previous studies, we focus on how the forcing of the background flow can produce distinctly different regional LF structures, structures that are strongly reminiscent of those identified by Kushnir & Wallace (1989) over the NH landmasses and oceans.

Longitudinal (zonal) variations in topography and diabatic heating are essential to producing realistic representations of the time-mean circulation of the atmosphere and oceans. Yet theoretical studies traditionally delegate the role of the external forcing to one of implicitness, wherein a zonally varying background flow is simply specified and its stability to disturbances subsequently examined. Such an approach is often born out of necessity, since the forcing structures that contribute to the time-mean flow are complex and difficult to represent, particularly in a way that isolates and makes transparent the underlying physics. Thus, specifying the background flow is often the only recourse to make progress in basic understanding. This approach is quite common and has been the cornerstone for a wide body of work that has sought to explain the origin of disturbances in the atmosphere and oceans (e.g. Pierrehumbert 1984; Kamenkovich & Pedlosky 1994; Li & Nathan 1997; Nathan 1997; Hodyss & Nathan 2004*b*).

Rather than specify the zonally varying background flow, we opt instead to specify the external forcing and systematically derive an expression for the spatial-temporal evolution of the total low-pass filtered flow. This approach obviates the need to formally specify, *a priori*, the background flow and disturbance fields; these fields fall out naturally from the development. Moreover, we are able to identify the distinct roles that the different external forcings impart to the local stability and structure of the flow. Theoretical progress relating external forcings to flow stability and structure has been hindered by the considerable mathematical difficulties posed by the zonally varying character of the flows.

Merkine (1982), Pierrehumbert (1983) and Andrews (1984) are examples of the few theoretical studies that have attempted to address how the nature of the forcing may impact the dynamics of large-scale geophysical flow. However, these studies centred mostly on disturbance stability rather than on disturbance regional structure. Although conservation laws have provided a theoretical framework for understanding

the broad connection between the zonally varying background flow and low-frequency instability (e.g. Swanson 2002), they have generally been applied to conservative flows, a restrictive condition that is generally not met in the real atmosphere. Moreover, explicit expressions relating growth rate and wave structure to the details of the background flow structure have for the most part remained elusive.

Apart from the unresolved theoretical issues, there also are several practical issues associated with understanding how the detailed nature of the forcings that produce the time-mean flow can affect extended-range weather forecasting and predictions of short-term climate variability. These issues hinge largely on the ability to predict the low-frequency field. In particular, inaccurate representation of the forcings that contribute to the climatological background flow may squelch certain low-frequency structures or misrepresent others. Such errors would result in reduced predictability on both intra-seasonal and interannual time scales.

With the above theoretical and practical issues in mind, and guided by Kushnir & Wallace's (1989) observational study of atmospheric LF variability, we formulate a simple barotropic model that allows us to focus on the physics that connects the stability of forced stationary long waves to the local development of LF instabilities. As we show later, the heart of the problem is intimately connected to the type of forcing that produces the stationary wave field and the nature of the LF instabilities – absolute or convective – that develop on the flow.

The paper is organized as follows. In § 2, we present the model and discuss the physical origin of the terms that govern the linear dynamics of the LF disturbance field. In § 3, we draw on conservation principles derived from Hamiltonian theory to provide a necessary condition for instability and a constraint on the allowable LF structures that can develop on Hamiltonian stationary waves. In § 4, we extend the Hamiltonian stability results of § 3 to non-Hamiltonian flows and demonstrate that two asymptotically similar stationary wave fields, one produced by topography and the other by a PV source, can produce qualitatively different LF instabilities. In § 5, we carry out a local stability analysis that connects the types of LF structure that emerge with the regional distribution of absolute instability and convective growth. The concluding remarks are given in § 6.

## 2. Low-frequency model

In contrast to the traditional approach of simply specifying the background flow, we specify the total external forcing. Once the total forcing is specified and partitioned into time-mean, zonal-mean and zonally varying components, we systematically derive the background flow. The portion of the background flow that arises solely from the time- and zonal-mean forcing is chosen such that it does not satisfy the classic Rayleigh inflection point criterion (background flows that satisfy Rayleigh's criterion for instability would produce a related evolution equation for the LF waves, e.g. Hodyss & Nathan 2004*c*) for instability (e.g. Pedlosky 1987 § 7.14). The portion of the background flow that arises from the seasonally and zonally varying forcing will constitute the seasonally and zonally varying stationary wave. The stability of the stationary wave and the characteristics of the LF instabilities that develop on it form the basis of our study. Symbolically, the streamfunction for the total LF portion of the flow can be written as,

$$\psi(x, y, t) = \underbrace{\bar{\psi}_0(y) + \varepsilon\bar{\psi}_1(y, t)}_{\substack{\text{Zonally}\\ \text{uniform flow}}} + \underbrace{\varepsilon\tilde{\psi}_1(x, y, t)}_{\substack{\text{Forced stationary}\\ \text{wave}}} + \underbrace{\varepsilon\tilde{\phi}_1(x, y, t)}_{\substack{\text{Low frequency}\\ \text{(free) wave}}}, \tag{2.1}$$

where $\varepsilon$ is a scaling parameter to be defined later, $(x, y)$ are distances in the zonal and meridional directions, and $t$ is time. The notation in (2.1) is non-conventional in the following sense. The overbar denotes the portion of the flow that arises from the zonal-mean *forcing*, not the zonal-mean of the *flow*. This distinction is important because the zonally varying portion of the flow, denoted by tildes, may also have zonal-mean components. Upon specifying the external forcing, each part of the total flow (2.2) will be systematically derived below.

### 2.1. *Model*

We consider a quasi-geostrophic barotropic model that is centred on a mid-latitude $\beta$-plane channel of infinite longitudinal (zonal) extent. (Owing to the channel sidewalls, which act as perfect reflectors, the LF waves may be meridionally resonant. Thus the LF wave amplitudes may be larger than they might otherwise be with open boundaries. However, Magnusdottir & Haynes (1999) have shown using a primitive equation model that under some conditions equatorward propagating planetary waves may be reflected from the subtropical zero wind line back into middle latitudes. This lends some support to the channel assumption without having to deal with the significantly more complicated meridionally open boundary problem.) The model fluid is bounded above by a rigid horizontal lid and below by broad spatially varying bottom topography. Large-scale diabatic heating is modelled by horizontal variations in an imposed potential vorticity (PV) source.

The model dynamics are governed by the quasi-geostrophic barotropic vorticity equation, which in the presence of topography, an external PV source and frictional (Ekman) damping can be written in the non-dimensional form (Pedlosky 1987):

$$\frac{\partial q}{\partial t} + J(\psi, q) = -r\nabla^2\psi + F. \tag{2.2}$$

In (2.2), $J(A, B) = A_x B_y - A_y B_x$ and $\nabla^2 = \partial^2/\partial x^2 + \partial^2/\partial y^2$; the geostrophic pressure (streamfunction) field is $\psi(x, y, t)$, which is related to the zonal and meridional wind fields $u = -\partial\psi/\partial y$ and $v = \partial\psi/\partial x$, respectively. The PV is $q = \nabla^2\psi + \beta y + h_B$; $\beta$ is the non-dimensional planetary vorticity gradient, and $h_B = h_B(x,y)$ is the localized bottom topography, which is assumed to vanish as $x \to \pm\infty$. The total external PV source is $F(x, y, t)$ and the parameter $r$ measures the Ekman damping strength.

The boundary condition at the channel sidewalls in a zonally infinite channel is $\psi = \bar{\psi}_0(y)$ at $y = -1,1$ (Helfrich & Pedlosky 1995). In the zonal direction, far from any localized forcing, the flow is zonally uniform and bounded such that $\psi(x \to \pm\infty, y, t) = \psi_\infty(y, t)$ and $\psi_\infty(y, t) < \infty$.

### 2.2. *Low-pass filtering*

The mathematical development used to obtain the governing equation for the LF wave field in (2.1) follows that in Hodyss & Nathan (2004*a*, hereinafter referred to as HN*a*). We employ the analytical counterpart to low-pass filtering of atmospheric data by introducing the long zonal scale $X = \varepsilon^{1/2}x$ and slow time scale $T = \varepsilon^{3/2}t$, for which the differential operators transform as $\partial/\partial x \to \varepsilon^{1/2}\partial/\partial X$ and $\partial/\partial t \to \varepsilon^{3/2}\partial/\partial T$, where $\varepsilon \ll 1$. To balance friction and external forcing with dispersion and nonlinearity, we scale the friction parameter as $r \to \varepsilon^{3/2}r$ and the external PV forcing as $F \to \varepsilon^{1/2}F$.

For $\varepsilon = 0.1$, the ratio of the zonal to meridional scales is $y/x \sim 0.3y/X$, which is consistent with observed low-frequency motions in the atmosphere (e.g. Hoskins, James & White 1983). For the same $\varepsilon$, the period $\tau_0 = O(\varepsilon^{-3/2}) \sim 32$, which, for characteristic wind and length scales of $U^* = 15$ m s$^{-1}$ and $L^* = 1000$ km, yields an advective time scale of about one month.

The low-pass field (2.1) is obtained by expanding the dependent variables in a perturbation series,

$$[\psi(X, y, T), q(X, y, T), F(X, y, T), h_B(X, y)] = \sum_{n=0}^{\infty} \varepsilon^n \left[\psi_n, q_n, \varepsilon^{1/2} F_n, h_n\right]. \tag{2.3}$$

Substituting (2.3) into (2.2) and equating like orders in $\varepsilon$ yield equations governing the components of the low-pass flow (2.1). Upon specifying the external forcings, each part of the total flow (2.2) will be derived systematically below. As in (2.1), we use an overbar to denote the portion of the flow that arises from the zonal-mean forcing and a tilde to denote the zonally varying portion of the flow.

The $O(1)$ zonal-mean flow is determined from a balance between the frictional damping and the $O(\varepsilon^{1/2})$ PV source, i.e. $-r\overline{\psi}_{oyy} = \bar{F}_1(y)$. The $O(\varepsilon)$ zonal-mean flow is the inhomogeneous solution to

$$\bar{\psi}_{1yy} - \Lambda_0 \bar{\psi}_1 = \bar{F}_r(y, T); \quad \bar{\psi}_1 = 0 \text{ at } y = -1, 1, \tag{2.4a}$$

where

$$\Lambda_0(y) = \frac{\partial \bar{Q}_0}{\partial \bar{\psi}_0} = -\frac{\bar{Q}_{0y}}{\bar{U}_0} \tag{2.4b}$$

is the $O(1)$ refractive index and $\bar{F}_r(y, T)$ is defined in Appendix A. To ensure that the instabilities that emerge are due solely to the imposed external forcing on the system, we restrict attention to the class of $O(1)$ zonal flows for which $\bar{Q}_{0y} \geqslant 0$, which ensures stability according to the Rayleigh criterion. For westerly flow, $\bar{Q}_{0y} \geqslant 0$ leads to a negative-definite refractive index (2.4*b*).

The $O(\varepsilon)$ stationary wave is the inhomogeneous solution to

$$\tilde{\psi}_{1yy} - \Lambda_0 \tilde{\psi}_1 = \frac{1}{\bar{U}_0} \int \tilde{F}_1(X, y, T)\, \mathrm{d}X - h_1, \tag{2.5}$$

where $\tilde{\psi}_1 = 0$ at $y = -1{,}1$. The structure of the stationary wave depends explicitly on the structure of the forcings on the right-hand side of (2.5). The stationary wave vanishes if the topography and PV source term balance, i.e. if $\tilde{F}_1 = \bar{U}_0 h_{1X}$. Because we are focusing on zonally localized stationary waves, the PV source, $\tilde{F}_1$, must have zero zonal mean. In contrast, any localized topography will produce a localized stationary wave.

The $O(\varepsilon)$ LF wave field can be written as

$$\tilde{\phi}_1(X, y, T) = A(X, T)\varphi(y), \tag{2.6}$$

where the meridional structure satisfies

$$\varphi_{yy} - \Lambda_0 \varphi = 0; \quad \varphi = 0 \text{ at } y = -1, 1. \tag{2.7}$$

Equation (2.7) states that, to lowest order, the meridional structure of the LF wave field is a free, stationary Rossby wave with local meridional wavenumber $\Lambda_0^{1/2}$.

At $O(\varepsilon^2)$, the stationary and LF waves interact to yield the LF amplitude equation,

$$A_T + \underbrace{\bar{m}_d A_{XXX} + m_p(X, T) A_X}_{\text{Net linear phase speed}} + \underbrace{m_g(X, T) A}_{\text{Linear growth}} + \underbrace{\bar{m}_n A A_X}_{\text{Nonlinearity}} = \underbrace{\tilde{f}(X, T)}_{\substack{\text{Rossby wave} \\ \text{source}}}, \tag{2.8}$$

where

$$m_p = \bar{m}_p(T) + \tilde{m}_p(X, T), \tag{2.9a}$$

$$m_g = r + \tilde{m}_g(X, T). \tag{2.9b}$$

The coefficients in (2.8) and (2.9) are defined in Appendix A. We note that HN*a* have used (2.8) as a model to examine the dynamics of solitary Rossby waves in zonally varying flow. They did not examine, however, the linear stability characteristics of (2.8) nor its general nonlinear dynamics. Here we focus on the former by considering the linear LF dynamics of flows that possess both absolute instability and local convective growth. The detailed analysis of the nonlinear LF dynamics described by (2.8) will be considered in Part 2 to this study.

The terms in (2.8) originate from the following terms in the barotropic vorticity equation (2.2):

$$\bar{U}_0\tilde{q}_X \Rightarrow \bar{m}_d A_{XXX}, \tag{2.10a}$$

$$J(\tilde{\phi}, \tilde{q}) \Rightarrow \bar{m}_n A A_X, \tag{2.10b}$$

$$U_1\tilde{q}_X + Q_{1y}\tilde{\phi}_X \Rightarrow [\bar{m}_p(T) + \tilde{m}_p(X, T)]A_X, \tag{2.10c}$$

$$\tilde{V}_1\tilde{q}_y - \tilde{Q}_{1X}\tilde{\phi}_y \Rightarrow \tilde{m}_g(X, T)A, \tag{2.10d}$$

$$\tilde{Q}_{1T} + J(\bar{\psi}_1 + \tilde{\psi}_1, \bar{Q}_1 + \tilde{Q}_1) - \bar{U}_0\tilde{Q}_{2X} + \tilde{F}_2 \Rightarrow \tilde{f}. \tag{2.10e}$$

Because the LF instabilities that develop on the stationary wave are so intimately connected to the coefficients and terms in (2.8–2.10), we review their physical origins. Different though complementary discussions of the coefficients can be found in HN*a* and Hodyss & Nathan (2006).

The linear dispersion term (2.10*a*) and the nonlinear advection term (2.10*b*) are unaffected by the interaction between the stationary and LF waves and thus have constant coefficients. The phase speed modulation term (2.10*c*) and the local growth rate term (2.10*d*), which both depend on the $O(\varepsilon)$ part of the background flow, have spatially and temporally varying coefficients that encapsulate the interaction between the stationary and LF waves. Because the LF wave is stationary to the $O(1)$ flow (see (2.7)), the LF characteristics of the free wave arise owing to dispersion (2.10*a*), the stationary wave (2.10*c*,*d*) and nonlinearity (2.10*b*).

The dispersion term (2.10*a*) can be shown to yield the classic expression for the zonal phase speed of a long low-frequency Rossby wave that is propagating on the $O(1)$ zonal-mean flow (Hodyss & Nathan 2004*b*, hereinafter referred to as HN*b*). The phase speed modulation term (2.10*c*) is an $O(\varepsilon)$ correction to the dispersion term; it involves the same linear advections that yield the classic Rossby phase frequency in the dispersion term. These advections are associated with meridional displacements of fluid parcels and, owing to the stabilizing influence of the $\beta$-effect, lead to neutral oscillations (Holton 2004, pp. 214–215). The phase speed modulation term (2.10*c*) consists of two parts. The first part, which is due to the $O(\varepsilon)$ zonal-mean flow, is chosen to cause the LF wave field to propagate slowly eastward, i.e. $\bar{m}_p > 0$. (The disturbance evolution when $\bar{m}_p < 0$ leads to other interesting dynamics, including Rossby wave tunnelling. This problem will be examined in a sequel to this work.) In the troposphere this is a reasonable assumption during the Northern Hemisphere winter, when the zonal-mean flow is relatively strong and the advection of disturbance relative vorticity dominates over the advection of background vorticity. The second part of the phase speed modulation term is due to the $O(\varepsilon)$ forced stationary wave. Depending on the detailed nature of the forcing structures that produce the stationary wave, the term $\tilde{m}_p(X, T)A_X$ may cause the LF wave to propagate eastward $[\tilde{m}_p(X, T) > 0]$ or westward $[\tilde{m}_p(X, T) < 0]$. Like the phase speed modulation term, the linear growth term (2.10*d*) involves advections; however, the advections that appear in the growth term are associated with longitudinal displacements of fluid parcels. As shown later, these

displacements result in either growth or decay of the disturbance field. The connection between longitudinal parcel displacements and disturbance growth is consistent with earlier work on non-zonal flows where it has been shown that fluid trajectories with a longitudinal component are less susceptible to the stabilizing influence of the $\beta$-effect and thus may be energy releasing (e.g. Pedlosky 1987, pp. 567–574).

The Rossby wave source $\tilde{f}(X, T)$ in (2.8) depends on both the $O(\varepsilon)$ stationary wave and the $O(\varepsilon^2)$ external forcing fields; the $O(\varepsilon)$ forcing fields contribute to $\tilde{f}(X, T)$ through their nonlinear interaction (see Appendix A, (A5)). For linearized waves, $\tilde{f}(X, T)$ would simply produce a forced solution to (2.8) and thus would have no effect on the linear stability problem considered here. Therefore, we set $\tilde{f}(X, T) = 0$, such that the stability is controlled solely by the stationary wave's *modulations* as measured by $\tilde{m}_p(X, T)$ and $\tilde{m}_g(X, T)$.

## 3. Conservation properties

In this section we focus on the Hamiltonian dynamics of the linearized LF evolution equation (2.8). Applying Hamiltonian methods to (2.8) yields several conservation properties, which provide a necessary condition for instability and a constraint on the allowable LF structures that can develop on Hamiltonian stationary waves. (Reviews of Hamiltonian methods applicable to fluid dynamics can be found in McIntyre & Shepherd 1987; Shepherd 1990; Salmon 1998.) Conservations laws for non-Hamiltonian stationary waves are briefly discussed in Appendix B.

### 3.1. *Hamiltonian dynamics*

The linearized LF amplitude equation (2.8) can be written as a Hamiltonian system of the form

$$A_T = -\frac{\partial}{\partial X}\left[\frac{\delta H}{\delta A}\right], \tag{3.1}$$

provided

$$\frac{\partial m_p}{\partial X} - m_g = -r - \frac{1}{R}\int_{-1}^{1} \frac{\partial}{\partial y}\left(\frac{\varphi}{\bar{U}_0}\tilde{F}_1\right)\frac{\varphi}{\bar{U}_0}\,\mathrm{d}y = 0. \tag{3.2}$$

In (3.1), $\delta H/\delta A$ is the functional derivative of the Hamiltonian, $H$, with respect to the LF amplitude, $A$, where the Hamiltonian is defined as,

$$H = \tfrac{1}{2}\int_{-\infty}^{\infty} \left(m_p A^2 - m_d A_X^2\right)\mathrm{d}X. \tag{3.3}$$

Because $\tilde{F}_1$ is zonally varying, (3.2) cannot be satisfied for viscous flow ($r \neq 0$). Hamiltonian flows must be inviscid ($r = 0$), which is our focus for the remainder of this section.

For inviscid flow, (3.2) shows that the evolution of the LF wave is Hamiltonian if the original asymptotic ordering of the external PV forcing is $F < O(\varepsilon^{3/2})$ or the PV source has a specific meridional structure. For example, if the PV source is symmetric and $\bar{U}_0$ is meridionally antisymmetric, then the system is Hamiltonian provided the LF wave is a meridional monopole. In contrast to the PV source, the system is Hamiltonian for any topographic forcing.

#### 3.1.1. *Integral invariants, stability and structure*

Equation (3.1) together with Noether's theorem allows for the identification of several integral invariants. For example, if the Hamiltonian (3.3) is invariant to

translations in $\alpha$, which may represent translations in either time or space, a functional $\Theta$ that satisfies

$$A_\alpha = \frac{\partial}{\partial X}\left[\frac{\delta \Theta}{\delta A}\right], \tag{3.4}$$

will be conserved.

The invariance of the Hamiltonian to translations in space ($\alpha = X$) yields the pseudomomentum, $P$, where

$$\Theta = P \equiv \tfrac{1}{2}\int_{-\infty}^{\infty} A^2 \, \mathrm{d}X \tag{3.5}$$

is conserved if $m_p$ varies only with time. Because the pseudomomentum is positive definite, time-varying zonally uniform flows are stable to long LF Rossby waves. Thus a necessary condition for LF instabilities is the existence of a stationary wave.

The invariance of the Hamiltonian to translations in time ($\alpha = T$) yields conservation of pseudoenergy, $E$, where $\Theta = E \equiv -H$. In this case, $m_p$ varies only in space, $X$. Because stationary waves produced by topography are clearly independent of time, the LF disturbances that develop on topographic stationary waves must conserve pseudoenergy. In contrast, stationary waves produced by PV sources must satisfy two conditions in order to produce LF disturbances that conserve pseudoenergy. The PV sources must be independent of time and have structures that satisfy (3.2).

Conservation of pseudoenergy provides a constraint on the types of flows that can support long LF instabilities. Because $m_d < 0$ for westerly flow (see Appendix A), a necessary condition for the instability of a Hamiltonian stationary wave is that $m_p(X)$ change sign somewhere in the domain. Further analysis of this stability condition (see Appendix C) shows that although the $O(1)$ parallel background flow we have considered is stable according to the Rayleigh criterion, it satisfies a necessary condition for instability due to Arnol'd's (1965) second theorem.

In steady zonally uniform flow, pseudoenergy and pseudomomentum must both vanish for instability. In steady zonally varying flow, only pseudoenergy must vanish for instability; the pseudomomentum is non-zero and modulated by the stationary wave, namely,

$$P_T = -\tfrac{1}{2}\int_{-\infty}^{\infty} \frac{\mathrm{d}\tilde{m}_p}{\mathrm{d}X} A^2 \, \mathrm{d}X. \tag{3.6}$$

Equation (3.6) states that in regions where $\tilde{m}_p$ increases (decreases), the LF amplitude decreases (increases). This means that a growing mode must be anchored to regions for which $\mathrm{d}\tilde{m}_p/\mathrm{d}X < 0$. Moreover, even when the pseudoenergy does not vanish and exponential instability is not possible, local convective growth can still occur as a wave travels through the zonally varying portion of the flow. Equation (3.6) states that a wave packet undergoing convective growth will have a permanent gain or loss in amplitude if the stationary wave field through which the packet is travelling is asymmetric.

The conservation of pseudomomentum and pseudoenergy can be supplemented with additional conservation laws by identifying Casimir invariants, $C$, that satisfy

$$\frac{\partial}{\partial X}\left[\frac{\delta C}{\delta A}\right] = 0, \tag{3.7}$$

where the Casimirs are essentially the 'homogeneous' solutions to (3.4). Thus the pseudomomentum and pseudoenergy can be defined only to within a Casimir of the

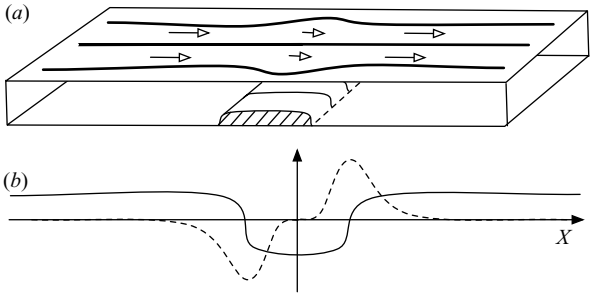


FIGURE 1. (*a*) Schematic rendering of the topographic landmass that produces a zonally varying streamfunction field. (*b*) The coefficients $m_p$ (solid) and $m_g$ (dashed) that are consistent with this streamfunction field are also shown.

system. Here we list only the Casimir invariant, 'mass', which is defined as

$$J = \int_{-\infty}^{\infty} A \, \mathrm{d}X. \tag{3.8}$$

Physically, the mass is the zonally uniform portion of the LF disturbance. Because mass is conserved, the zonally integrated amplitude must vanish for unstable waves. Thus the LF instabilities that develop on Hamiltonian flows must have oscillatory structures.

## 4. Some explicit results

In this section, we present some explicit stability results for both Hamiltonian and non-Hamiltonian background flows that are time-independent and governed by the linearized LF equation (2.8). We demonstrate that two asymptotically similar stationary wave fields, one produced by topography and the other by a PV source, can produce qualitatively different LF instabilities. Doing so extends earlier work by Merkine (1982), Pierrehumbert (1983) and Andrews (1984), who noted that the nature of the forcing that produces a stationary wave may impact its stability. They did not address, however, the broader issues surrounding the role that different external forcings play in producing forced zonally varying flows that spawn different low-frequency structures in different regions.

### 4.1. *Forcing structures and coefficients*

The two types of stationary waves that we consider are intense jets or split flows that are independent of time. Figure 1(*a*) gives a schematic rendering of the broad topography that produces a zonally varying streamfunction field. A schematic rendering of the coefficients, $m_p$ and $m_g$, that is consistent with this streamfunction field is also shown.

The zonally localized, $O(\varepsilon)$ topography is chosen as

$$h_1(X, y) = M(y)\mathrm{Z}(X), \tag{4.1}$$

where

$$\mathrm{Z}(X) = \tfrac{1}{2}\begin{cases} 1 + \tanh(X + X_h) & (X \leqslant 0), \\ 1 - \tanh(X + X_h) & (X > 0). \end{cases} \tag{4.2}$$

In (4.2), $2X_h$ measures the zonal width of the topography. The zonal structure is chosen to be a wide shallow mount of unit amplitude, which is qualitatively similar

to a broad continental landmass. By inserting (4.1) into the forced stationary wave equation (2.5), we obtain

$$\tilde{\psi}_1(X, y) = Z(X)\Phi(y), \tag{4.3}$$

where the meridional structure function, $\Phi(y)$, is the particular solution to

$$\Phi_{yy} - \Lambda_0\Phi = -M, \qquad \Phi(\pm 1) = 0. \tag{4.4}$$

We have solved (4.4) for physically relevant topographic forcing and found meridional monopole and dipole structures, which are consistent with the observed structures of atmospheric LF variability. To consider the effects of a broad range of forcing structures on the stability of the flow, we leave $M(y)$ arbitrary and consider various combinations of $m_p(X)$ and $m_g(X)$.

The zonally localized PV source is chosen as

$$\tilde{F}_1(X, y) = -\bar{U}_0 M \frac{\mathrm{d}Z}{\mathrm{d}X}. \tag{4.5}$$

Insertion of (4.5) into (2.5) yields the stationary wave structure (4.3), the same wave structure that was produced by the topography. Yet, as shown below, these two stationary waves, which are identical to $O(\varepsilon)$ but originate from different forcings, can yield LF instabilities that are completely different.

The coefficients $\tilde{m}_p(X)$ and $\tilde{m}_g(X)$ in (2.9), which control the types of LF instabilities that develop, depend on the details of how the stationary wave is forced. This is made clear if the stationary wave (4.3) is inserted into the expressions for $\tilde{m}_p(X)$ and $\tilde{m}_g(X)$, i.e.

$$\tilde{m}_p(X) = N_p Z, \quad \tilde{m}_g(X) = N_g \frac{\mathrm{d}Z}{\mathrm{d}X}, \tag{4.6a, b}$$

where

$$N_p = \frac{1}{R}\int_{-1}^{1} [\Lambda_{0y}\Phi\varphi - \alpha M_y \varphi]\frac{\varphi}{\bar{U}_0}\,\mathrm{d}y, \tag{4.7a}$$

$$N_g = \frac{1}{R}\int_{-1}^{1} [\Lambda_{0y}\Phi\varphi + \alpha M \varphi_y]\frac{\varphi}{\bar{U}_0}\,\mathrm{d}y, \tag{4.7b}$$

where $\alpha = 0$ for topographically forced flow and $\alpha = 1$ for PV forced flow. As in the discussion of the amplitude coefficients in § 2, the constants $N_p$ and $N_g$, respectively, determine the effects of the stationary wave on the linear propagation and local growth of the LF wave field. For stationary waves forced solely by topography, the second term in (4.7*a*, *b*) is absent so that $N_p = N_g$, a parameter setting for which the flow is Hamiltonian, whereas for stationary waves forced solely by PV, $N_p \neq N_g$. In addition, it can be shown that for meridionally uniform $O(1)$ flow (4.7*a*) and (4.7*b*) are always related by $N_p = 2N_g$. As shown below, differences between $N_p$ and $N_g$ control the differences in the types of LF instabilities that develop on topographic or PV forced stationary waves.

### 4.2. *Oscillatory modes versus envelope modes*

The LF instabilities that develop on various forced stationary waves are obtained by numerically solving the linearized form of (2.8) using a pseudospectral method with the third-order Adams–Bashforth scheme in time. The spectral expansion is truncated at 128 Fourier modes. Periodic and non-periodic conditions were imposed at the upstream and downstream boundaries with no significant difference in the numerical results. The numerical results presented below are based on the non-periodic conditions, which we model by imposing a damping region at the upstream

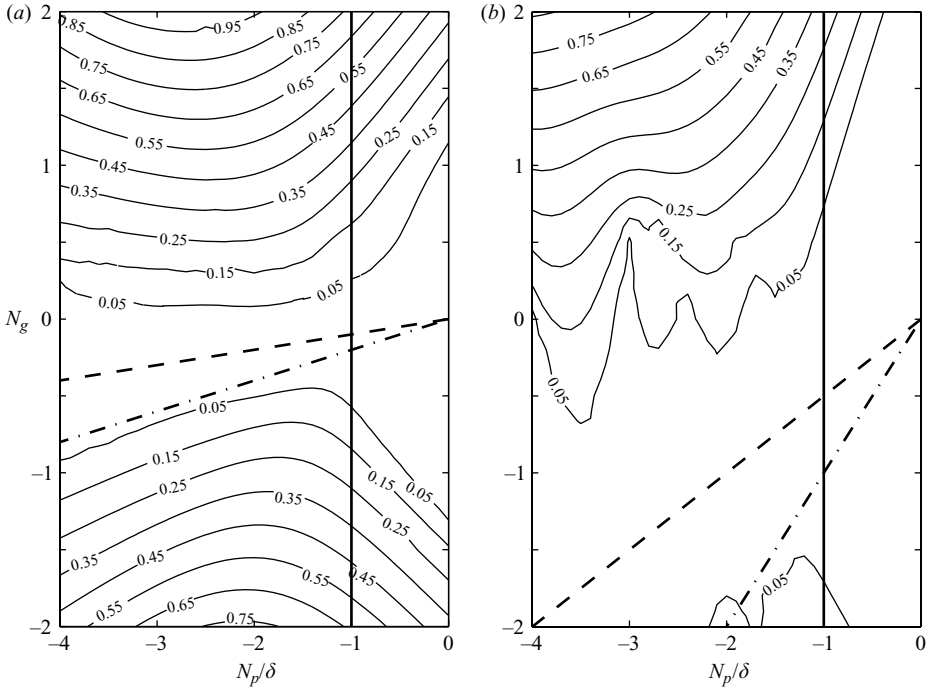


FIGURE 2. The growth rate in the $N_p$ versus $N_g$ plane for (*a*) $\delta = 0.2$ and (*b*) $\delta = 1.0$. The stability diagram divides into an oscillatory mode region and an envelope mode region, which are separated by the (dashed) neutral stability curve. The dashed-dotted line denotes the line in parameter space for which the topographic stationary waves exist. To the left of the solid vertical line $m_p$ changes sign and to the right it does not.

and downstream boundaries. The initial condition is small-amplitude random noise and the flow is assumed inviscid. The model is integrated forward in time until the most unstable mode dominates the solution.

To ease comparison with the WKB analysis to be presented in § 5, we define a scaling parameter $\delta$, such that $\bar{m}_d = -\delta^3$, $\bar{m}_p = \delta$, $\tilde{m}_g(X) = N_g \mathrm{d}Z/\mathrm{d}X$ and $\tilde{m}_p(X) = N_p Z = \delta n_p Z$, where $n_p$ is introduced to make explicit the dependence of $N_p$ on the scaling factor $\delta$. The WKB limit corresponds $\delta \ll 1$. For the results to be presented below, the zonal width parameter is $X_h = 5$ and the zonal structure is given by (4.2). Zonal widths larger and smaller than $X_h = 5$ and a variety of zonal structures different from (4.2) were also examined; in all cases there were two distinct LF solution basins. As described below and elaborated upon in § 5, one basin is characterized by oscillatory structures and the other by envelope modes.

Figure 2 shows the growth rate in the $N_p$ versus $N_g$ plane for $\delta = 0.2$ and $\delta = 1$. For both cases, the stability diagram divides into two distinct regions: (*a*) an oscillatory mode region and (*b*) an envelope mode region. The modal structures for each region are shown in figure 3. The oscillatory and envelope mode regions in figure 2 are separated by the (dashed) neutral stability curve, which is defined in Appendix B. The growth rate maximum that occurs in the upper (lower) left portion of figures 2(*a*) and 2(*b*) corresponds to envelope (oscillatory) modes. The envelope (oscillatory) modes occur for $N_g > 0$ ($<0$). The envelope modes generally have a much greater growth rate than the oscillatory modes. The dashed-dotted line denotes the line in parameter space along which the entire family of Hamiltonian stationary

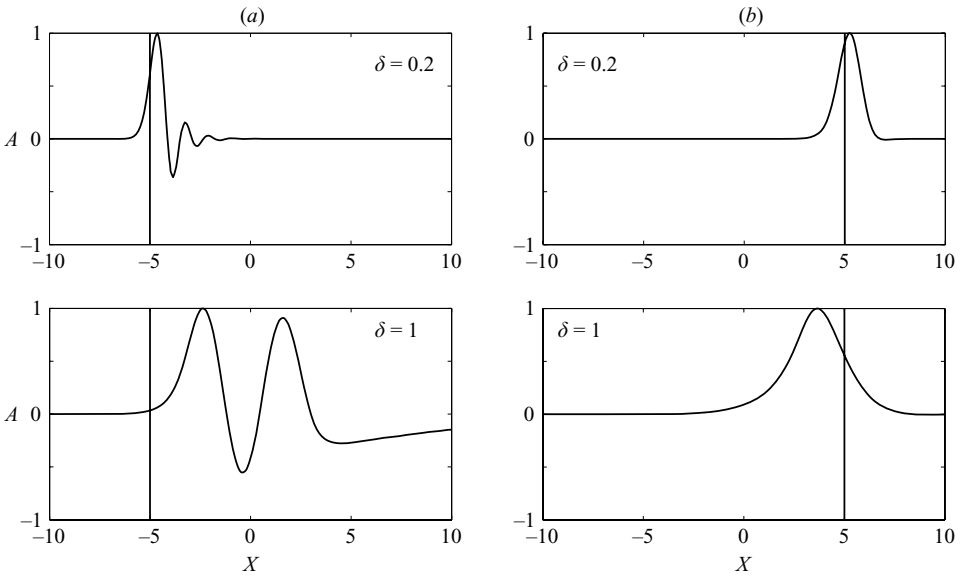


FIGURE 3. The structures of the (*a*) oscillatory and (*b*) envelope modes for the two values of $\delta$ used in figure 2.

waves exists. By plotting the growth rate in the $(N_p, N_g)$ plane, we have collapsed the Hamiltonian portion of phase space to a single line, a line along which much of the previous work on geophysical flows has been focused. Compared to the PV stationary waves, the Hamiltonian stationary wave instabilities are so weak that they fall below the resolution of the contours. Consistent with the Hamiltonian results of § 3, the instability of the Hamiltonian stationary waves occurs to the left of the vertical line, i.e. where $m_p$ changes sign. In contrast to the Hamiltonian stationary waves, the PV stationary waves are unstable even where $m_p$ does not change sign. In addition, recall that $O(1)$ flows that are meridionally uniform always satisfy $N_p = 2N_g$, a parameter setting which is always stable.

Figure 3 shows the structures of the oscillatory and envelope modes for the two values of $\delta$ used in figure 2. Generally, for both modal structures, as $\delta$ increases, the disturbance wavenumber decreases and the penetration into the downstream far field increases. The vertical line in each figure, along which $m_p = 0$, corresponds to a divergent group velocity field, an important point that is discussed further in the following section.

## 5. Local stability analysis

The Hamiltonian analysis of § 3 provided a necessary condition for instability and a constraint on the allowable structures that can develop on Hamiltonian flows. Section 4, which considered both Hamiltonian and non-Hamiltonian flows, provided detailed numerical results that underscore the importance of knowing the origin of the stationary wave in order to predict the low-frequency structures that develop.

In this section, we carry out a local linear stability analysis of (2.8) for background flow that is time-independent and non-Hamiltonian. The analysis explains the emergence of the oscillatory and envelope structures in terms of the regional distribution of absolute instability and convective growth. The formal mathematical

procedure that distinguishes absolute instability from convective growth is given by Briggs (1964), who examined plasma instabilities in plane parallel flows. The Briggs procedure was first applied in a geophysical context by Merkine (1977) for parallel flow and later by Pierrehumbert (1984) and Bar-Sever & Merkine (1988) for weakly non-parallel flow. Much of the more recent work involving the local stability of zonally varying flow has centred on the complex linearized Ginzburg–Landau equation (CLGL), which is of second order in the zonal coordinate (e.g. Le Dizes *et al.* 1996; Huerre & Rossi 1998). In a fluid dynamical context, the CLGL provides a relatively simple framework to examine the local stability of flows for which the zonally uniform far field satisfies the Rayleigh criterion for instability. In contrast to the CLGL, the linearized LF equation (2.8) is of third order, has real coefficients, and is based on a flow for which the zonally uniform far field does not satisfy the Rayleigh criterion for instability.

The response of a zonally varying flow to an initial disturbance field may manifest itself in one of four ways (e.g. Huerre & Rossi 1998): absolute instability (AI), convective growth (CG), neutrality, or stability. If the initial disturbance excites a growing wave of zero group velocity, which consequently grows without bound at every point in space, the flow is said to be *absolutely unstable*. If the initial disturbance field propagates and grows locally only at fixed points in space, decaying or remaining neutral elsewhere, the flow is said to be *convectively unstable*. If the initial disturbance field neither grows nor decays at all fixed points in space, the flow is said to be *neutral*. If the initial disturbance field decays at all fixed points in space, the flow is said to be *stable*.

The major distinction between AI and CG is that a localized region of AI exhibits dynamics that are intrinsic to the system, whereas a localized region of CG only serves as a spatial amplifier of remotely forced wave trains. As shown below, distinct regions along the flow may be identified that are absolutely unstable, convectively unstable, neutral or stable. The distribution and zonal extent of these individual regions, which are controlled by the external forcing, plays a central role in determining the regional structure of the LF wave.

### 5.1. *WKB analysis*

In this sub-section, we employ a WKB formalism and derive explicit expressions for the growth rates and structures for both the absolutely unstable and convectively unstable disturbances. We focus on inviscid flow in regions of parameter space where the low-frequency wave is weakly dispersive [$m_d = O(\delta^3)$] and slowly propagating [$m_p(X) = O(\delta)$] (this parameter setting is tantamount to assuming that the stationary wave is slowly varying, which could also be made explicit by setting $\chi = \delta X$, where $\delta \ll 1$ measures the ratio of the scale of the LF wave to that of the stationary wave). In order to ensure instability at lowest order we assume $m_g(X) = O(1)$.

For this parameter setting, we search for normal-mode solutions to (2.8) of the form

$$A(X, T) = a(X) \exp[-\mathrm{i}(\omega_0 + \delta\omega_1 + \ldots)T] + \text{c.c.}, \tag{5.1}$$

where $\omega$ is the complex frequency. The spatially modulated amplitude is expanded in WKB form (Bender & Orszag 1978),

$$a(X) = \exp\left(\frac{S_0(X;\omega_0)}{\delta} + S_1(X;\omega_1) + \cdots\right), \tag{5.2}$$

where the $S_j(X;\omega_j)$ control the amplitude and phase modulation of the wave. Insertion of (5.1) and (5.2) into (2.8) yields, for the first two terms in (5.2),

$$a(X) = \exp\left(\frac{\mathrm{i}}{\delta}\int^X k_0\,\mathrm{d}X' + \int^X \frac{\mathrm{i}\omega_1 + 3m_d k_0 k_{0X'}}{c_g}\,\mathrm{d}X'\right), \tag{5.3}$$

where

$$D(k_0,\omega_0;X) \equiv m_d k_0^3 - m_p k_0 + \omega_0 + \mathrm{i}m_g = 0 \tag{5.4}$$

is the dispersion relation and

$$c_g = m_p - 3m_d k_0^2 \tag{5.5}$$

is the corresponding lowest-order group velocity. (Because we have assumed that the stationary wave is weak, the dispersion relation (5.4) is considerably simpler than in previous work (e.g. Pierrehumbert 1984).) The local zonal wavenumber, $k_0(X,\omega_0)$, is defined by $S_{0X}(X;\omega_0) = \mathrm{i}k_0(X;\omega_0)$.

5.1.1. *Absolute instability*

In the WKB framework, a necessary condition for normal mode instability is the existence of a localized region of absolute instability, where the maximum absolute growth rate serves as the upper bound on the normal mode growth rate (Pierrehumbert 1984; Huerre & Rossi 1998). For a given zonally varying flow, the procedure for determining the normal mode frequency pivots on determining the branch points in the complex $X$-plane. If the branch points are off the real axis, the one closest to the real axis is the most physically relevant (Boyd 1999).

We begin with the dispersion relation (5.4), which is a cubic polynomial in $k_0(X;\omega_0)$, where $k_0$, $X$ and $\omega$ each may be complex. Each of the three roots for $k_0(X;\omega_0)$ corresponds to a branch of the dispersion relation, with each branch yielding an LF wave of the form (5.3). Because the forced stationary wave decays to zero as $X_r \to \pm\infty$, two conditions follow: (i) the LF wave must also decay to zero as $X_r \to \pm\infty$ and (ii) a single branch of the dispersion relation must satisfy $k_0(-\infty;\omega_0) = k_0(\infty;\omega_0)$. In addition, for the LF wave to decay to zero as $X_r \to \pm\infty$, we require that the $\mathrm{Im}(k_0)$ be positive as $X_r \to \infty$ and negative as $X_r \to -\infty$. Assume two branches of (5.4) cross at the *branch point*, $X_0$, such that

$$k_0^L(X_0;\omega_0) = k_0^R(X_0;\omega_0), \tag{5.6}$$

where the branch point may be complex. Here, $k_0^L$ is the branch to the left of $X_0$, where $\mathrm{Im}(k_0^L) < 0$ as $X_r \to -\infty$, and $k_0^R$ is the branch to the right of $X_0$, where $\mathrm{Im}(k_0^R) > 0$ as $X_r \to \infty$. Clearly, a single (root) branch of the dispersion relation cannot simultaneously satisfy both the upstream and downstream boundary conditions; therefore branch switching must occur somewhere in the domain. A branch point is classified as a square root branch point if two of the roots of the dispersion relation (5.4) coalesce at the branch point. Similarly, a branch point is classified as a cube root branch point if three of the roots of the dispersion relation coalesce at the branch point.

Given (5.6), it follows that the dispersion relation has a complex saddle point such that

$$\left.\frac{\partial D}{\partial k_0}\right|_{X=X_0} = 0 \Rightarrow c_g(X_0) = 0. \tag{5.7}$$

Therefore, branch points correspond to those points along the flow where the complex group velocity vanishes.

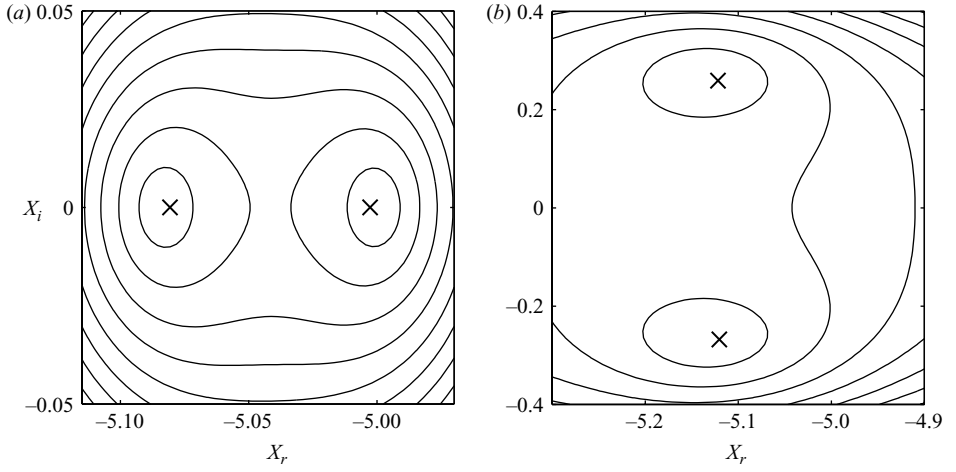


FIGURE 4. The branch points in the complex $X$-plane for $N_g = -2$ (oscillatory mode), $N_p = -2$ (figure 4*a*) and $N_p = -3$ (figure 4*b*) are denoted by the '×'. The contours denote the function $F_{br}$, which monotonically decreases towards the branch points.

The differential of the dispersion relation (5.4) and the group velocity relation (5.7) together yield a formula that defines the position of the branch point. The differential of (5.4) can be written as

$$\frac{\mathrm{d}D}{\mathrm{d}X} = \frac{\partial D}{\partial X} + \frac{\partial D}{\partial k_0}\frac{\partial k_0}{\partial X} = 0. \tag{5.8}$$

Applying (5.8) at the branch point and using (5.7) yields

$$\left.\frac{\partial D}{\partial X}\right|_{X=X_0} = 0, \tag{5.9}$$

which, when combined with (5.4), yields the local zonal wavenumber at the branch point, namely,

$$k_0(X_0, \omega_0) = \mathrm{i}\frac{\mathrm{d}m_g/\mathrm{d}X}{\mathrm{d}m_p/\mathrm{d}X}. \tag{5.10}$$

Using (5.10) in (5.7) yields an equation that defines the locations of the branch points, namely,

$$F_{br}(X_0) = m_p\left(\frac{\mathrm{d}m_p}{\mathrm{d}X}\right)^2 + 3m_d\left(\frac{\mathrm{d}m_g}{\mathrm{d}X}\right)^2 = 0. \tag{5.11}$$

Using (5.10) and (5.11) and evaluating (5.4) at the branch point yields the leading-order approximation to the normal mode frequency:

$$\omega_0 = \mathrm{i}\left(m_d\left[\frac{\mathrm{d}m_g/\mathrm{d}X}{\mathrm{d}m_p/\mathrm{d}X}\right]^3 + m_p\frac{\mathrm{d}m_g/\mathrm{d}X}{\mathrm{d}m_p/\mathrm{d}X} - m_g\right)\Bigg|_{X_0}. \tag{5.12}$$

Figure 4 shows $F_{br}$ and the branch points for $N_g = -2$ (oscillatory mode), $N_p = -2$ (figure 4*a*) and $N_p = -3$ (figure 4*b*). In figure 4(*a*), the branch points are on the real axis, where the right-hand one is a cube-root branch point and the left-hand one is a square-root branch point. For both branch points, the $\mathrm{Re}(\omega_0) = 0$ and the $\mathrm{Im}(\omega_0) = 1.0$. The left-hand branch point, however, does not satisfy (5.6) (i.e. neither of the two branches that pinch at the branch point vanish as $X_r \to -\infty$) and is thus

neglected. Figure 4(*b*) shows a pair of square-root branch points that are located symmetrically about the $X_r$-axis. In this case, the branch points are associated with equal growth rates $\mathrm{Im}(\omega_0) = 0.92$ but different frequencies; $\mathrm{Re}(\omega_0) = -0.095$ for the one where $X_\mathrm{i} > 0$ and $\mathrm{Re}(\omega_0) = 0.095$ for the one where $X_\mathrm{i} < 0$. Because these two branch points are equally dominant, they must be linearly superposed to represent the normal mode instability. Linearly superposing two waves with equal and opposite real frequency leads to a standing oscillation, which is confirmed by the numerical solutions of § 4. The branch-point configurations described here are consistent with Le Dizes *et al.*'s (1996) characterization of the instabilities in the complex Ginzburg–Landau equation; specifically, we find instabilities associated with one double branch point on the real axis or two single branch points off the real axis which are connected by a common Stokes line.

Our numerical results show that irrespective of whether the branch points are real or complex, only two structures emerge – oscillatory modes or envelope modes. Thus for ease of discussion, we focus on the conceptually simpler case of real branch points and consider the cube-root branch point shown in figure 4(*a*).

The real branch point on the right in figure 4(*a*) can be shown to satisfy the three conditions for a cube-root branch point: (i) $D(k_0, \omega_0; X_0) = 0$, (ii) $\partial D/\partial k_0 = 0$, and (iii) $\partial^2 D/\partial k_0^2 = 0$ (Bender & Orszag 1978, § 7.5). The existence of a cube-root branch point, however, makes choosing the appropriate branch of the solution ambiguous. To remove the ambiguity, the standard procedure is to introduce some additional physics that has been omitted from the dispersion relation (5.4). Here, we add a small amount of nonlinearity. Before doing so, however, consider the dispersion relation (5.4), which is based on the linearized form of (2.8). At the branch point the dispersion relation yields, for $m_p = 0$ and $\omega_0 = -\mathrm{i}m_g$, a condition on the wavenumber, i.e. $k_0^3 = 0$. Thus, the three roots for $k_0$ coalesce at the branch point when $m_p = 0$. This suggests that introducing some additional physics that leads to propagation across the branch point will eliminate the ambiguity. Now consider the nonlinear equation (2.8), where we note that the nonlinear term is simply an amplitude-dependent phase speed term. Combining $m_p A_X$ with $m_n A A_X$ in (2.8) yields a modified phase speed modulation term, $m_p A_X \rightarrow (m_p + m_n A) A_X$, which is non-zero at the branch point. Thus the amplitude of the wave, no matter how small, yields a non-vanishing phase speed modulation term at the branch point. Consequently, the cube-root branch point does not survive in the presence of small, yet finite amplitude waves. We, in fact, obtain a square-root branch point, meaning only two roots coalesce at the branch point – these two roots are then matched to form the leading-order WKB approximation.

Figure 5 shows the leading-order WKB solution for the most unstable normal mode that develops on the PV forced stationary wave of § 4.1. The parameters are: $\delta = 0.2$, $N_p = -2$, $N_g = 2$ (envelope mode), $N_g = -2$ (oscillatory mode). Both modes have the same lowest-order frequency, $\omega_0 = i$. Figure 6 presents a comparison between the WKB and numerically determined estimates of the growth rate as a function of $\delta$. Note that in the limit as $\delta \rightarrow 0$ the growth rate asymptotes to the WKB estimate.

Comparison of the WKB solutions in figure 5 with the numerically determined solutions in figure 3 show only small phase differences between the modes. These small phase differences would be reduced by including the next order term, $S_1(X,\omega_1)$, in the WKB solution (5.3). The calculation of $S_1(X,\omega_1)$ is in principle straightforward, although in practice quite lengthy. In particular, $S_1(X,\omega_1)$ is singular at the branch point, which invalidates the expansion (5.2). The singular perturbation problem must then be solved by matching the (inner) solution in the vicinity of the branch point with the (outer) solution far from the branch point. Matching the inner and outer

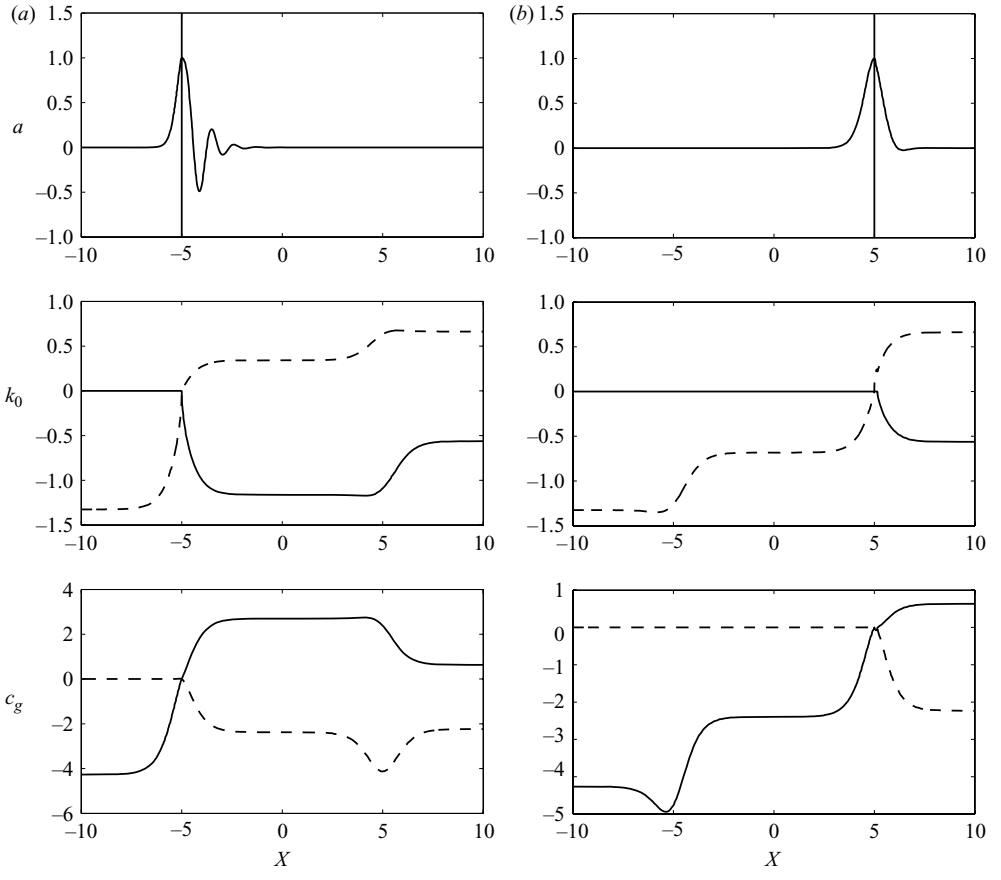


FIGURE 5. The leading-order WKB solution for the most unstable mode that develops on the PV forced stationary wave of §4.1. The parameters are: (*a*) $\delta = 0.2$, $N_p = -2\delta$, $N_g = -2$ (oscillatory mode), (*b*) $N_g = 2$ (envelope mode).

solutions yields the frequency correction $\omega_1$ and thus $S_1(X,\omega_1)$ (see, for example, Bar-Sever & Merkine 1988). Fortunately, $S_1(X, \omega_1)$ does not have to be calculated to capture the basic physics of the normal mode instabilities; the leading-order WKB solution is adequate.

Pierrehumbert (1984) noted, within the context of baroclinic instability, that a conceptual picture of the normal mode instabilities can be formed from the perspective of absolute instability, whereby a branch point is associated with a wave *source*. This picture, which carries over to the barotropic forced wave problem considered here, hinges on the following. Emanating from a branch point are two waves, each associated with a different branch of the dispersion relation (5.4). One branch, $k_0^R$, is associated with a wave that propagates to the right and vanishes as $X_r \to \infty$. The other branch, $k_0^L$, is associated with a wave that propagates to the left and vanishes as $X_r \to -\infty$. This conceptual picture is consistent with figure 5, where a divergent group velocity field exists at the branch point.

### 5.1.2. *Convective growth*

To determine regions of convective growth, we check each point in $X$ for a ray with real wavenumber along which a travelling wave has positive growth rate. If such a

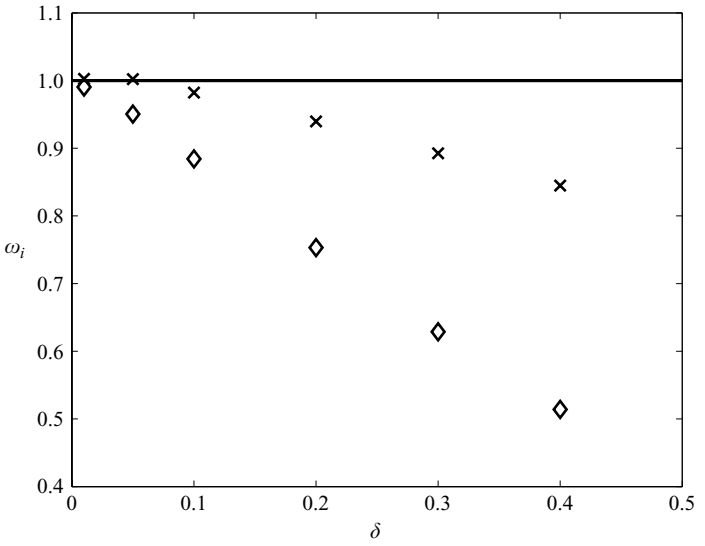


FIGURE 6. Numerically determined growth rate as a function of $\delta$. $\diamond$, values for the oscillatory mode in figure 5($a$); $\times$, values for the envelope mode in figure 5($b$). The horizontal line denotes the leading-order WKB estimate of the growth rate. Note that the growth rates for both the oscillatory and envelope modes asymptote to the WKB estimate as $\delta \to 0$.

point exists and the flow is absolutely stable there, we label that point in the flow as convectively unstable.

We define a ray at the position, $X_c$, moving at the speed, $V$, such that $c_g(X_c) = V$. From (5.5) we see that $m_p < c_g$ for real, non-zero wavenumber, defined by $k_0(X_c) = \pm\sqrt{(m_p - V)/3m_d}$. Using this expression for $k_0(X_c)$, the dispersion relation (5.4) yields the frequency for the wave propagating along the ray:

$$\omega_0(X_c) = \tfrac{1}{3}k_0(X_c)[2m_p + V] - \mathrm{i}m_g. \tag{5.13}$$

Because $k_0(X_c)$ is real, (5.13) shows that the spatial distribution of convective growth follows the spatial distribution of $m_g(X) = r + \tilde{m}_g(X)$. For the idealized stationary waves of § 4, which are symmetric about $X = 0$, an incoming wavetrain convectively grows where $m_g < 0$ and convectively decays where $m_g > 0$.

Gaster (1962) has shown that in the limit of weak growth rate the local convective growth can be interpreted as either local temporal growth or as local spatial growth, with the respective growth rates related by the Gaster transformation $\omega_{0\mathrm{i}} \approx -k_{0\mathrm{i}}c_{gr}$. We have verified that this transformation holds for the convectively unstable waves in this model. The transformation does not hold for the absolute instabilities because $c_g = 0$ at the branch point. Using the Gaster transformation, the net convective growth, $G$, of a wavetrain propagating in from infinity is given at a position, $X$, by

$$G(X) = \exp\left(-\frac{1}{\delta}\int_{-\infty}^{X} k_{0\mathrm{i}}\,\mathrm{d}X'\right) \approx \exp\left(\frac{1}{\delta}\int_{-\infty}^{X} \frac{\omega_{0\mathrm{i}}}{c_{gr}}\,\mathrm{d}X'\right). \tag{5.14}$$

Equation (5.14) shows that slowly propagating wavetrains undergo the largest convective growth. Because $\omega_{0\mathrm{i}} = -m_g$, the structure of the stationary wave, as manifest through its meridional wind distribution, strongly influences the resulting convective growth. The degree of asymmetry of the stationary wave about $X = 0$ determines the amount of energy an incoming wavetrain gains or loses upon exiting

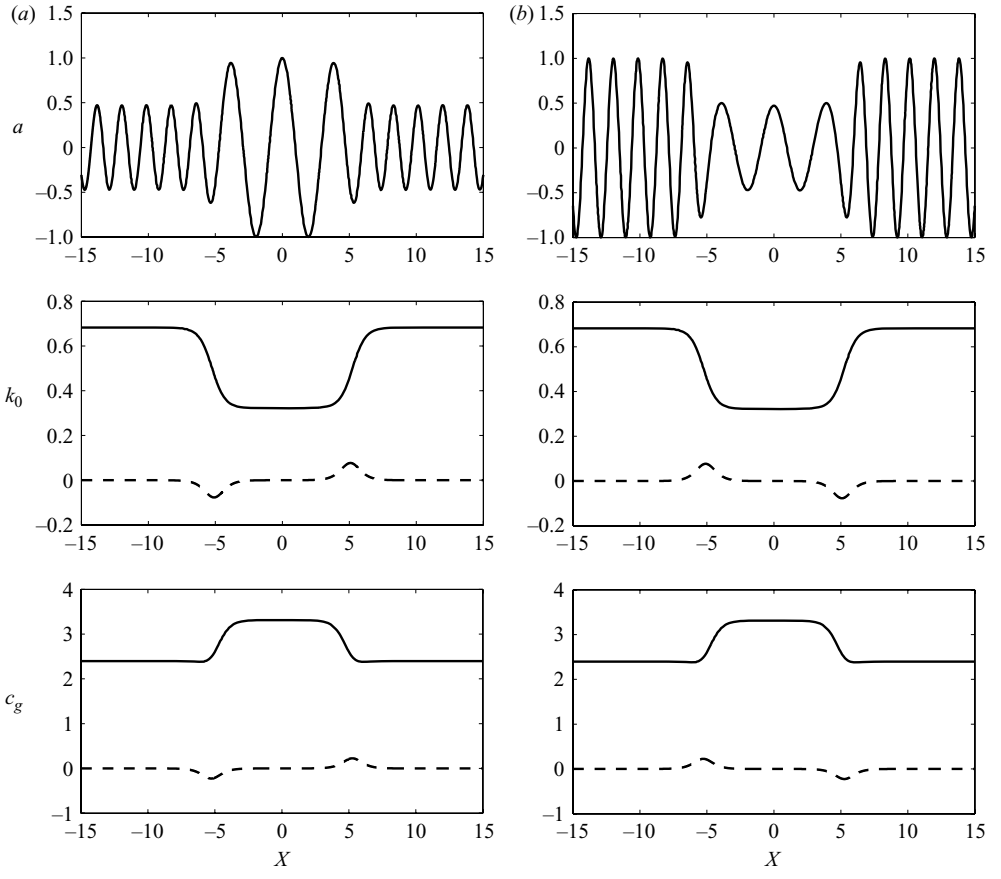


FIGURE 7. An example of (*a*) upstream and (*b*) downstream convective growth in a flow that is free of absolutely instability. The parameters are: (*a*) $\delta = 0.2$, $N_p = 2\delta$, $N_g = 0.4$; (*b*) $N_g = -0.4$.

the stationary wave region. Ekman damping ($r \neq 0$) introduces an asymmetry in $m_g$, leading to a net loss of energy as a wavetrain propagates through the stationary wave region.

Depending on the type of streamwise boundary condition that is imposed, the convective growth induced by an *asymmetric* stationary wave may exhibit distinct differences. For example, radiation boundary conditions will lead to a finite amount of convective growth as the wave traverses the stationary wave region (see (5.14)). In contrast, periodic boundary conditions will lead to continual convective growth as the wave periodically enters and exits the stationary wave region. Because the absolute instabilities are non-propagating and strongly localized, only convective growth regions can lead to instabilities that require the periodic recycling of energy (e.g. Pierrehumbert 1984).

Figure 7 shows an example of upstream and downstream convective growth in a flow that is free of absolutely instability. The parameters are: $\delta = 0.2$, $N_p = 2$, $N_g = \pm 0.4$. In the upstream far field, we introduce an eastward propagating wave train with $\omega_0 = 1$. As the wave train propagates through the stationary wave, local growth (decay) occurs where $m_g(X) < 0$ ($m_g(X) > 0$).

### 5.2. *Regional distribution of absolute instability and convective growth*

In this sub-section we provide a geometric interpretation of the closely related spatial and temporal instability theories in order to determine the regional distribution of absolute instability and convective growth.

Temporal branches are associated with complex frequency and real wavenumber, whereas spatial branches are associated with complex wavenumber and real frequency (Huerre & Rossi 1998 and references therein). Consider the algebraic dispersion relation $D(k_0, \omega_0; X) = 0$ given by (5.4). When (5.4) is evaluated for real wavenumber $k_0$, there is a single complex frequency $\omega_0$ that corresponds to temporal instability for $\omega_{0i} = -m_g > 0$. When (5.4) is evaluated for real frequency, there are three wavenumber solutions, each corresponding to a different spatial branch. Although one or more of these branches may appear to exhibit spatial growth (i.e. for an eastward moving wave $-k_i > 0$), this growth may in fact be spurious (e.g. Briggs 1964). To formally determine the physically relevant spatial growth, the initial-value problem must be solved. The initial-value approach is in principle straightforward, but in practice technically difficult. Fortunately, based on early work by Briggs (1964), among others, Pierrehumbert (1986) and Huerre & Rossi (1998) have shown that by examining the geometry of the spatial branches, the regions of absolute instability and convective growth can easily be determined. The geometric approach hinges on examining, for real frequency, the variations of the (complex) spatial branches with variations in a control parameter, say, $X$. If a branch crosses the $k_i = 0$ axis but does not pinch with another branch, the flow is convectively unstable. On the other hand, if a branch crosses the $k_i = 0$ axis and pinches with another branch, the flow is absolutely unstable. Figure 8 shows the geometry of the spatial branches for four different values of $X$ (the control parameter) for the stationary wave that supports the oscillatory mode shown in figure 3. For each $X$, the branches were obtained by varying the frequency. Figure 8($a$) shows, for $X = -\infty$, where the flow is zonally uniform, the branch geometry for neutral flow – no roots cross the $k_i = 0$ axis. In figure 8($b$), where $X = -6.3$, the middle branch approaches but does not pinch with the lower branch, which is indicative of convective growth. In figure 8($c$), where $X = -6.1$, the branch that approached the lower branch in figure 8($b$) has pinched with the lower branch to form two lower branches. This branch geometry is associated with absolute instability. It is important to note that in figures 8($b$) and 8($c$) the branch which is immediately below the $k_i = 0$ axis never crosses the $k_i = 0$ axis, which means there is no long or short wave cutoff; all real wavenumbers have positive temporal growth rate, as verified by (5.13). Figure 8($d$) shows, for $X = 0$, the geometry of the branches for the transition from absolute growth to absolute decay. For this branch geometry, the flow is neutral. Because the stationary wave that we are considering is symmetric about $X = 0$, in the region $X > 0$ the branches in figures 8($a$)–8($c$) are merely mirrored about the $k_i = 0$ axis. This mirroring means that the approaching and/or pinching of the branches occurs above the $k_i = 0$ axis. Thus in the $X > 0$ region, the geometry of the spatial branches can be shown to correspond to spatial decay and thus temporal decay; the flow is stable for $X > 0$.

Applying the aforementioned procedure to determine the regional branch geometries of the four stationary waves above produces figure 9. Figure 9($a$) (figure 9$b$) is for the stationary wave that contains an absolutely unstable region that would give rise to an oscillatory (envelope) mode. For the oscillatory (envelope) mode, the branch point is upstream (downstream) of the stationary wave centre. This is the key difference between the oscillatory and envelope modes. The wave source region (i.e. branch point) for the oscillatory mode emits a downstream branch that must

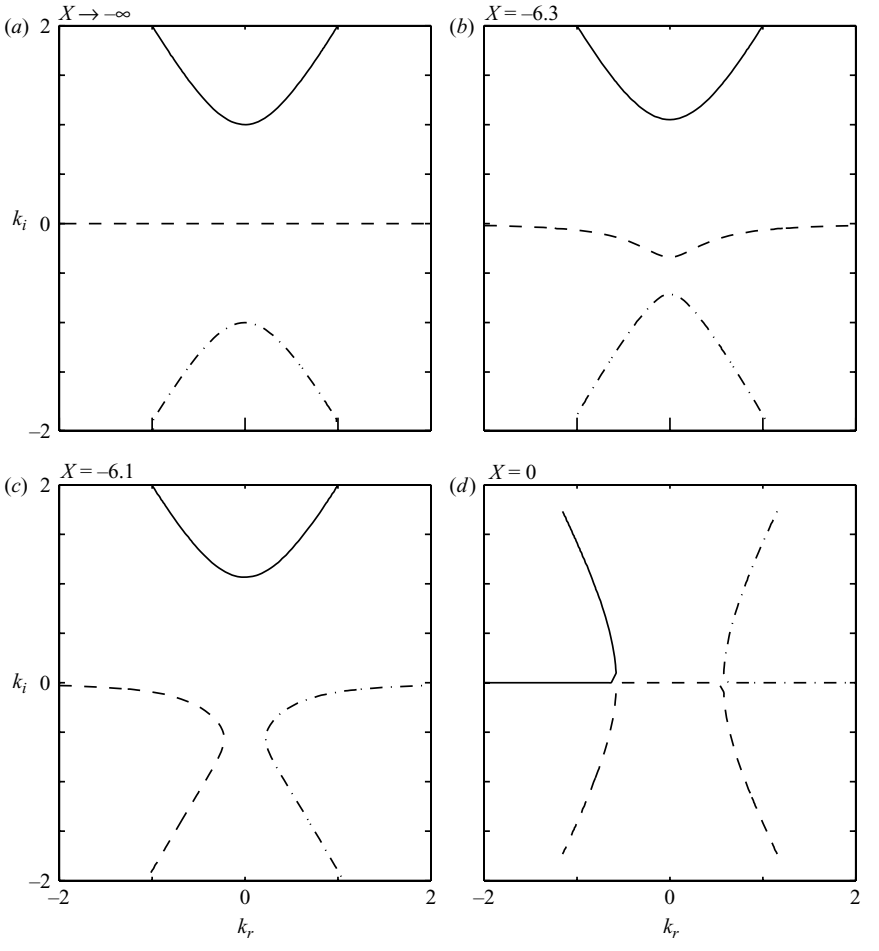


FIGURE 8. The geometry of the spatial branches for four different values of $X$ for the stationary wave that supports the oscillatory mode shown in figure 5.

propagate through a region of absolute instability and then immediately into a region of stability. In contrast, the wave source region for the envelope mode emits a downstream branch that remains in the absolutely unstable region for only a short time before it enters the convectively unstable region.

Figures 9($c$) and 9($d$) show the distribution of stability properties for stationary waves that are convectively unstable but free of absolute instability. Because the convective growth regions are on opposite sides of the stationary wave fields depicted in figures 9($c$) and 9($d$), the local growth characteristics are quite different. In figure 9($c$) (figure 9$d$) an incoming wavetrain grows (decays) as it propagates into the upstream side of the stationary wave field and decays (grows) as it propagates out of the downstream side. In both cases, the wavetrain returns to its initial amplitude because the stationary wave field is symmetric about $X = 0$.

## 6. Concluding remarks

The role of topography and potential vorticity sources in controlling the local linear stability of stationary long waves to long low-frequency (LF) Rossby waves has been

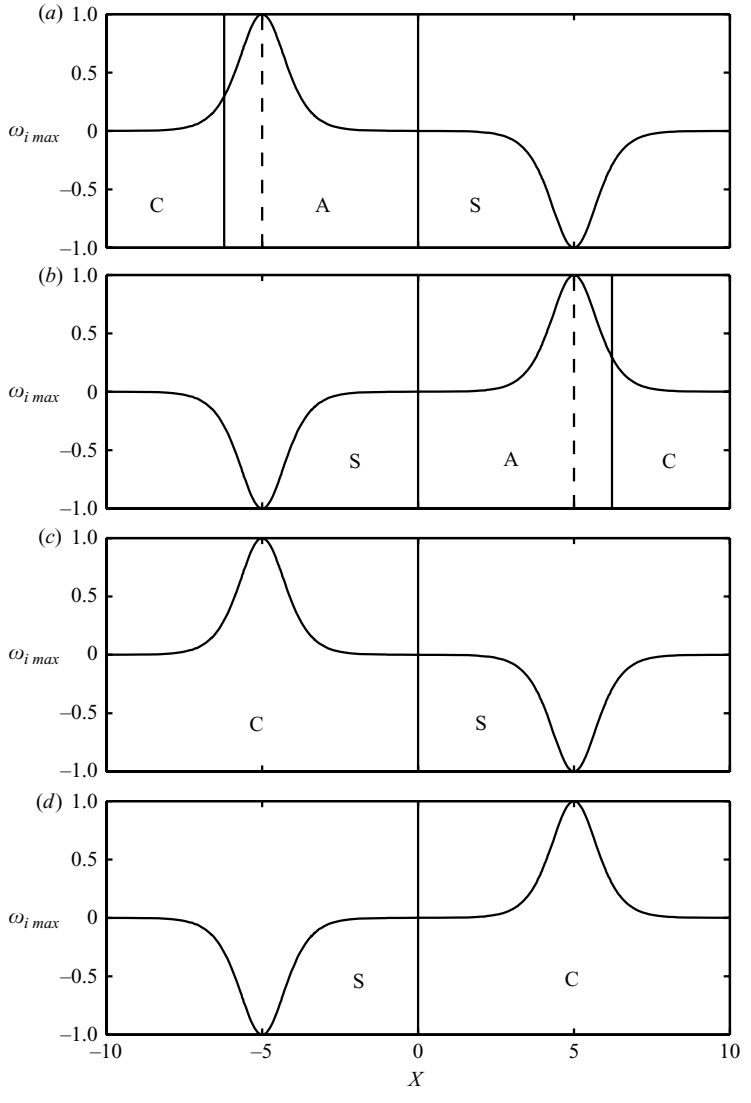


FIGURE 9. The regional distribution of absolute instability (A) and convective growth (C) for four different stationary waves. S indicates stable. The vertical solid lines denote the boundaries separating the various stability regions. Plots $(a, b)$ show the stationary wave that contains an absolutely unstable region that would give rise to $(a)$ an oscillatory and $(b)$ an envelope mode. Plots $(c, d)$ show an incoming wave train that $(c)$ grows and $(d)$ decays as it propagates into the upstream side of the stationary wave field and decays (grows) as it propagates out of the downstream side. Also shown in each figure is the curve of maximum temporal growth rate. The dashed line denotes the location of the branch point.

examined using a quasi-geostrophic barotropic model. By drawing on conservation principles derived from Hamiltonian theory, numerical results obtained from a set of systematically derived LF flow equations, and a local WKB analysis of absolute instability and convective growth, we have derived explicit stability criteria and constraints on the LF structures that can develop on stationary long waves.

The LF evolution equation (2.8) pivots on a background flow which, in the absence of stationary waves, is stable according to the classic Rayleigh criterion. Although the

$O(1)$ parallel background flow is 'Rayleigh stable', we show that it satisfies a necessary condition for instability that is related to Arnol'd's (1965) second theorem for the stability of plane curvilinear flow. We resolve this apparent paradox by showing that any amount of zonal variation in the background flow may render the flow unstable to long LF waves with stationary meridional wavenumber.

Explicit knowledge of the forcing that produces the stationary waves is shown to be crucial to predicting a unique LF field. Specific examples are given where various topographies or external potential vorticity (PV) sources can be chosen that produce stationary waves that differ by asymptotically small amounts, yet the LF instabilities that emerge may manifest themselves in strikingly different ways. If the stationary wave field is forced solely by topography, LF streamwise oriented wave trains always emerge. In contrast, if the stationary wave field is forced solely by PV, two LF structures are possible: streamwise elongated envelope modes or streamwise oriented wavetrains. To our knowledge, the development of the envelope modes is new, and represents a novel means for generating coherent structures within the context of a linear LF theory.

The LF dynamics of the model are shown to be Hamiltonian for any topographic forcing and for PV forcing having special structure. For such forcing, conservation laws for pseudoenergy, pseudomomentum and 'mass' are derived that yield necessary conditions for instability and constraints on the allowable LF structures that can develop on forced stationary waves. We show, for example, that Hamiltonian LF instabilities cannot arise from time variations in the background flow alone, but require streamwise variations in the background flow. When the Hamiltonian LF instabilities do arise, they must have zero-mean in the streamwise direction.

Analysis of the absolute and convective instability properties of the flow allows us to predict the type and location of the low-frequency structures that can develop on stationary waves. The problem hinges on identifying, via a WKB analysis, the locations of the complex branch points of the flow, which anchor the absolute instability. If the absolute instability region is on the upstream side of the stationary wave field, LF, streamwise oriented wavetrains emerge. If the absolute instability region is on the downstream side of the stationary wave field, LF, envelope (non-oscillatory) modes emerge.

For flows that are free of absolute instabilities, LF wavetrains originating in the zonally uniform far field can locally amplify via convective growth induced by the streamwise variations of the stationary wave. If the flow is inviscid and the stationary wave is symmetric about a longitude, the wavetrain exits the stationary wave region with the same amplitude that it had when it entered the region. If the flow is viscous and/or the stationary wave is asymmetric, then a wavetrain entering the stationary wave region will exit the region with different amplitude. Factors that can produce asymmetry in the stationary wave include (i) a symmetric PV source or asymmetric topography, (ii) a non-zonal jet axis produced by non-zonal forcing structures and (iii) a combination of PV sources and topography.

The successful simulation of atmospheric LF variability will depend in part on the accurate depiction of the location of the energy source for the LF instability, a point that has also been noted by Merkine (1982). In addition, we have shown here that the instability and structure of the LF wave will depend on an extremely fine-scale feature – the complex branch point derived from the WKB analysis. Moreover, the amplitude of the LF wave has been shown to be controlled by the meridional wind distribution of the underlying stationary wave. For rapidly growing modes, the branch point must be co-located with the maximum in the temporal growth rate.

Thus, successful simulation of atmospheric LF variability will depend on the accurate representation of the structure of the stationary wave, and consequently on the forcing from which the stationary wave originated.

The theory developed here should have applicability to a broad-range of atmospheric and oceanic phenomena characterized by long LF features. For example, the LF structures that develop on the stationary wave fields analysed here are reminiscent of the low-frequency structures observed by Kushnir & Wallace (1989) in the northern hemisphere troposphere during winter. They show slowly modulated wavetrains over the broad continental landmasses and zonally elongated features over the oceans (see their figures 5 and 8). Their 'continental modes' are similar to the oscillatory modes that emerge from the topographically forced stationary waves, while their 'oceanic modes' are similar to the envelope modes that emerge from the PV forced stationary waves. Although Kushnir & Wallace suggest that both mode types are consistent with remote forcing from the tropics, our theory provides an alternative explanation for the generation of continental and oceanic modes.

Part 2 to this study will address the nonlinear dynamics of the oscillatory and envelope modes discovered here. There are good reasons to believe that these two distinct modes will equilibrate in fundamentally different ways. For example, for topographic stationary waves, for which the flow is Hamiltonian, 'mass' is conserved irrespective of disturbance amplitude, meaning the disturbances that emerge must have zero zonal-mean. Thus, the oscillatory modes will not alter the zonal-mean flow. In contrast, because the PV stationary waves do not conserve 'mass', alterations to the zonal-mean flow can be expected, even in regions far-removed from the external PV forcing. Moreover, to what extent the linear structures obtained here preserve their integrity at finite-amplitude remains to be seen.

The authors thank Professors Ray Pierrehumbert, John Boyd and Michael Brown, as well as two anonymous reviewers, for their insightful comments on several aspects of this work. D. H. was supported by a Rosenstiel Postdoctoral Fellowship from the University of Miami. T. N. was supported in part by NASA grant LWS04-0025-0108.

## Appendix A. Definition of the coefficients in (2.8)

The forcing in (2.4$a$) is obtained by combining the $O(\varepsilon)$ and $O(\varepsilon^2)$ zonal-mean balances:

$$\bar{F}_r(y,T) = [-\bar{U}_{1y}(y,0) - \Lambda_0(\bar{\psi}_1(y,0) - [\bar{U}_1(-1,T) - \bar{U}_1(-1,0)](y+1))]\mathrm{e}^{-rT} + \mathrm{e}^{-rT}\int_0^T \frac{\bar{F}_2}{\bar{U}_0}\mathrm{e}^{r\tau}\,\mathrm{d}\tau + \int_{-1}^{y}\mathrm{e}^{-rT}\left(\int_{-1}^{y}\int_0^T \frac{\bar{F}_2}{\bar{U}_0}\mathrm{e}^{r\tau}\,\mathrm{d}\tau\,\mathrm{d}y'\right)\mathrm{d}y, \tag{A 1}$$

where $\bar{\psi}_1(y,0)$ is the initial zonal-mean structure, $\bar{U}_1(-1,0)$ is the initial boundary zonal wind, and $\bar{U}_1(-1,T)$ is the boundary zonal wind at time $T$.

The coefficients and inhomogeneous forcing term in (2.8) are partitioned into zonally uniform (overbar) and zonally varying (tilde) parts:

$$\bar{m}_d = \frac{1}{R}\int_{-1}^{1}\varphi^2\,\mathrm{d}y, \tag{A 2$a$}$$

$$\bar{m}_n = \frac{1}{R}\int_{-1}^{1}\Lambda_{0y}\frac{\varphi^3}{\bar{U}_0}\,\mathrm{d}y \tag{A 2$b$}$$

$$\bar{m}_p(T) = \frac{1}{R}\int_{-1}^{1} [\Lambda_0 \bar{U}_1 + \bar{Q}_{1y}]\frac{\varphi^2}{\bar{U}_0}\,\mathrm{d}y, \tag{A 3a}$$

$$\tilde{m}_p(X,T) = \frac{1}{R}\int_{-1}^{1} [\Lambda_0 \tilde{U}_1 + \tilde{Q}_{1y}]\frac{\varphi^2}{\bar{U}_0}\,\mathrm{d}y \tag{A 3b}$$

$$\tilde{m}_g(X,T) = \frac{1}{R}\int_{-1}^{1} [\tilde{V}_1(\Lambda_0\varphi)_y - \tilde{Q}_{1X}\varphi_y]\frac{\varphi}{\bar{U}_0}\,\mathrm{d}y, \tag{A 4}$$

$$\tilde{f}(X,T) = -\frac{1}{R}\int_{-1}^{1} [\tilde{Q}_{1T} + J(\bar{\psi}_1 + \tilde{\psi}_1, \bar{Q}_1 + \tilde{Q}_1) - \bar{U}_0\tilde{Q}_{2X} + \tilde{F}_2]\frac{\varphi}{\bar{U}_0}\,\mathrm{d}y, \tag{A 5}$$

where

$$R = -\int_{-1}^{1} \frac{\bar{Q}_{0y}}{\bar{U}_0^2}\varphi^2\,\mathrm{d}y. \tag{A 6}$$

Equation (A6) is the Rayleigh inflection point integral in the long-wave and low-frequency limit. Because we are considering $O(1)$ zonal-mean flows for which the $O(1)$ potential vorticity gradient is positive, R $< 0$.

In (A2)–(A5), the background PV gradients are given by

$$\bar{Q}_{1y}(y,T) = -\bar{U}_{1yy}, \tag{A 7}$$

$$\tilde{Q}_{1y}(X,y,T) = -(\tilde{U}_{1yy} - h_{1y}), \tag{A 8}$$

$$\tilde{Q}_{1X}(X,y,T) = \tilde{V}_{1yy} + h_{1X}, \tag{A 9}$$

$$\tilde{Q}_{2X}(X,y,T) = \tilde{V}_{1XX} + h_{2X}, \tag{A 10}$$

where the subscripts 1 and 2 denote $O(\varepsilon)$ and $O(\varepsilon^2)$ quantities, respectively.

## Appendix B. Dynamics of non-Hamiltonian flows

For arbitrary, time-independent stationary waves the equations for pseudoenergy, pseudomomentum and mass contain sources and sinks, i.e.

$$E_T = \int_{-\infty}^{\infty}\left(\frac{\mathrm{d}m_p}{\mathrm{d}X} - m_g\right)[m_p A^2 + m_d A A_{XX}]\,\mathrm{d}X, \tag{B 1a}$$

$$P_T = \int_{-\infty}^{\infty}\left(\frac{\mathrm{d}m_p}{\mathrm{d}X} - 2m_g\right)A^2\,\mathrm{d}X, \tag{B 1b}$$

$$J_T = \int_{-\infty}^{\infty}\left(\frac{\mathrm{d}m_p}{\mathrm{d}X} - m_g\right)A\,\mathrm{d}X. \tag{B 1c}$$

Equation (B1*b*) shows that stationary wave fields satisfying

$$\frac{\mathrm{d}m_p}{\mathrm{d}X} - 2m_g = 0 \tag{B 2}$$

are stable. Equation (B2), which defines the neutral stability curve in figure 2, is satisfied only for stationary waves forced by PV.

Equation (B1*c*) shows that for non-Hamiltonian stationary waves, (3.2) is not satisfied. Consequently, the disturbance has non-zero zonal-mean, meaning that envelope modes may emerge (see the numerical results in § 4 and the WKB results in § 5). Assuming $A > 0$, growth of the disturbance amplitude $A$ will depend strongly on the extent to which it projects onto the region where $(\mathrm{d}m_p/\mathrm{d}X - m_g) > 0$. Thus,

significant growth can be anticipated if the structure of $A$ is similar to the structure of $\mathrm{d}m_p/\mathrm{d}X - m_g$. Because the envelope modes will generally project more strongly onto the structure of the growth region than the oscillatory modes, it follows that the envelope modes will generally have larger growth rates.

## Appendix C. Pseudoenergy and Arnol'd's second theorem

The pseudoenergy-derived stability condition obtained in § 3 can be related to Arnol'd's (1965) stability theorem for plane curvilinear flow (a lucid exposition of Arnol'd's theorem can also be found in Pedlosky 1987, § 7.17). Below we prove two corollaries: (i) there is a simple relationship between the coefficient $m_p$ in (2.8) and the refractive index $\Lambda$ of the background flow; (ii) the invariant of Arnol'd's (1965) second theorem reduces here to the pseudoenergy constraint obtained in § 3.

The first corollary may be proved by appealing to the definition of the refractive index:

$$\Lambda = \frac{\partial Q}{\partial \Psi} = \frac{V Q_x - U Q_y}{U^2 + V^2}, \tag{C 1}$$

where $\Psi$, $Q$, $U$ and $V$, represent, respectively, the background streamfunction, potential vorticity, and zonal and meridional wind fields. We begin by expanding (C 1) in an asymptotic series in $\varepsilon$,

$$\Lambda = \Lambda_0 + \varepsilon \Lambda_1 + \cdots \tag{C 2}$$

and use (2.1) to obtain

$$\Lambda_0 = -\frac{\bar{Q}_{0y}}{\bar{U}_0}, \tag{C 3a}$$

$$\Lambda_1 = -\left[\bar{U}_1 + \tilde{U}_1 + \frac{\bar{Q}_{1y} + \tilde{Q}_{1y}}{\bar{Q}_{0y}} \bar{U}_0\right] \frac{\bar{\Lambda}_0}{\bar{U}_0}. \tag{C 3b}$$

Equation (C 3$b$) allows $m_p$ to be written as

$$m_p = -\frac{1}{R} \int_{-1}^{1} \Lambda_1 \varphi^2 \mathrm{d}y \tag{C 4}$$

Because we have shown that a change in sign of $m_p$ is a necessary condition for instability, (C 4) shows that this is equivalent to a change in sign of $\Lambda_1$. Because $R < 0$, stability is assured when $\Lambda_1 \geqslant 0$.

To prove the second corollary, we must relate (C 4) to Arnol'd's (1965) second theorem. We start from the Arnol'd invariant, which for the present model takes the form

$$\frac{\mathrm{d}}{\mathrm{d}t} \int_{-\infty}^{\infty} \int_{-1}^{1} \left[E + \frac{\zeta^2}{2\Lambda}\right] \mathrm{d}x \, \mathrm{d}y = 0, \tag{C 5}$$

where $E = (\tilde{\phi}_x^2 + \tilde{\phi}_y^2)/2$ is the kinetic energy, $\zeta = \tilde{\phi}_{xx} + \tilde{\phi}_{yy}$ is the relative vorticity, and $\tilde{\phi} = \tilde{\phi}(x, y, t)$ is the disturbance streamfunction. Equation (C 5) shows that a sufficient condition for stability is $\Lambda > 0$; therefore a necessary condition for instability is $\Lambda < 0$.

Recall from § 2, our $O(1)$ background flow is such that $\bar{U}_0 > 0$ and $Q_{0y} \geqslant 0$; it follows that $\Lambda_0 < 0$. Therefore, the $O(1)$ parallel background flow is stable according to the Rayleigh criterion; yet the same parallel background flow satisfies a necessary condition for instability according to Arnol'd's second theorem. We show below that the zonal variation in the background flow (which is neglected by the Rayleigh

criterion) may render the flow unstable to long zonal waves with stationary meridional wavenumber.

Because we are focusing on long low-frequency waves, we impose a long $x$-scale on the disturbance field such that $\partial/\partial x \to \varepsilon^{1/2}\partial/\partial X$, insert (C 2) into (C 5), and balance like orders in $\varepsilon$. The lowest-order balance yields

$$\frac{\mathrm{d}}{\mathrm{d}t}\int_{-\infty}^{\infty}\int_{-1}^{1}\left[\tilde{\phi}_y^2 + \frac{\tilde{\phi}_{yy}^2}{\Lambda_0}\right]\mathrm{d}X\,\mathrm{d}y = 0, \tag{C 6}$$

which shows that this integral must vanish for instability. This integral will vanish for waves with stationary meridional wavenumber, i.e. $\Lambda_0^{1/2}$. This can be shown by using (2.7) in (C 6) and integrating by parts. Hence, $O(1)$ zonal flows for which $Q_{0y} \geqslant 0$ and $\Lambda_0 < 0$ are marginally stable to long waves with stationary meridional wavenumber. Because this flow is marginally stable, rather than deeply stable, an $O(\varepsilon)$ change to the flow may lead to instability. Hence, Rayleigh's criterion is not broadly applicable to geophysical flows with any amount of zonal variation.

At the next order, we obtain

$$\frac{\mathrm{d}}{\mathrm{d}t}\int_{-\infty}^{\infty}\int_{-1}^{1}\left[\frac{1}{2}\tilde{\phi}_X^2 + \frac{\tilde{\phi}_{yy}}{\Lambda_0}\phi_{XX} - \frac{1}{2}\frac{\tilde{\phi}_{yy}^2}{\Lambda_0^2}\Lambda_1\right]\mathrm{d}X\,\mathrm{d}y = 0. \tag{C 7}$$

Using (2.7) in (C 7) and integrating by parts allows (C 7) to be written as

$$\frac{\mathrm{d}}{\mathrm{d}t}\int_{-\infty}^{\infty}\int_{-1}^{1}\left[\Lambda_1\tilde{\phi}^2 + \tilde{\phi}_X^2\right]\mathrm{d}X\,\mathrm{d}y = 0. \tag{C 8}$$

Thus, in agreement with analysis of $m_p$ given above, instability requires that $\Lambda_1$ change sign; stability is assured when $\Lambda_1 \geqslant 0$. Agreement between (C 8) and the Hamiltonian definition (3.3) can be shown by using $\tilde{\phi} = A(X, T)\varphi(y)$ in (C 8). Thus, flows that satisfy the Rayleigh criterion for stability may be rendered unstable by the addition of $O(\varepsilon)$ non-parallel flow, and this instability will take the form of a long wave with stationary meridional wavenumber.

## REFERENCES


Andrews, D. G. 1984 On the stability of forced non-zonal flows. *Q. J. R. Met. Soc.* **110**, 657–662.

Arnol'd, V. I. 1965 Conditions for nonlinear instability of stationary plane curvilinear flows of an ideal fluid. *Dokl. Akad. Nauk. SSSR* **162**, 975–978. (Engl. transl. *Sov. Math.* **6**, 773–777, 1965.)

Bar-Sever, Y. & Merkine, L. O. 1988 Local instabilities of weakly non-parallel large-scale flows: WKB analysis. *Geophys. Astrophys. Fluid Dyn.* **41**, 233–286.

Bender, C. M. & Orszag, S. A. 1978 *Advanced Mathematical Methods for Scientists and Engineers.* McGraw–Hill.

Boyd, J. P. 1999 The Devil's Invention: Asymptotic, Superasymptotic and Hyperasymptotic Series. *Acta Appl. Maths.* **56**, 1–98.

Briggs, R. J. 1964 *Electron-Stream Interaction with Plasmas*, pp. 8–46. MIT Press.

Charney, J. & Eliassen, A. 1949 A numerical method for predicting the perturbations of the middle latitude westerlies. *Tellus* **1**, 38–54.

Gaster, M. 1962 A note on a relation between temporally increasing and spatially increasing disturbances in hydrodynamics instability. *J. Fluid Mech.* **14**, 222–224.

Held, I. M., Ting, M. & Wang, H. 2002 Northern winter stationary waves: theory and modeling. *J. Climate* **15**, 2125–2144.

Helfrich, K. R. & Pedlosky, J. 1995 Large-amplitude coherent anomalies in baroclinic zonal flows. *J. Atmos. Sci.* **52**, 1615–1629.

Hodyss, D. & Nathan T. R. 2004*a* Effects of topography and potential vorticity forcing on solitary Rossby waves in zonally varying flow. *Geophys. Astrophys. Fluid Dyn.* **98**, 175–202.

Hodyss, D. & Nathan, T. R. 2004*b* The connection between coherent structures and low-frequency wave packets in large-scale atmospheric flow. *J. Atmos. Sci.* **61**, 2616–2626.

Hodyss, D. & Nathan, T. R. 2004*c* Long waves in streamwise varying shear flows: new mechanisms for a weakly nonlinear instability. *Phys. Rev. Lett.* **93**, 074502.

Hodyss, D. & Nathan, T. R. 2006 Instability of variable media to long waves with odd dispersion relations. *Commun. Math. Sci.* **4**, 669–676.

Holton, J. R. 2004 *An Introduction to Dynamic Meteorology*. Academic.

Hoskins, B. J., James, I. N. & White, G. H. 1983 The shape, propagation and mean-flow interaction of large-scale weather systems. *J. Atmos. Sci.* **40**, 1595–1612.

Huerre, P. & Rossi, M. 1998 Hydrodynamic instabilities in open flows. In *Hydrodynamics and Nonlinear Instabilities* (ed. C. Goldrèche & P. Manneville), pp. 81–294. Cambridge University Press.

Kamenkovich, I. V. & Pedlosky, J. 1994 Instability of baroclinic currents which are locally non-zonal. *J. Phys. Oceanogr.* **51**, 2418–2433.

Kushnir, Y. & Wallace, J. 1989 Low-frequency variability in the northern hemisphere winter: geographical distribution, structure and time-scale dependence. *J. Atmos. Sci.* **46**, 3122–3142.

Le Dizes, S., Huerre, P., Chomaz, J. M. & Monkewitz, P. A. 1996 Linear global modes in spatially developing media. *Phil. Trans. R. Soc. Lond.* A **354**, 169–212.

Li, L. & Nathan, T. R. 1997 Effects of low-frequency tropical forcing on intraseasonal tropical–extratropical interactions. *J. Atmos. Sci.* **54**, 332–346.

McIntyre, M. E. & Shepherd, T. G. 1987 An exact local conservation theorem for finite-amplitude disturbances to non-parallel shear flows, with remarks on Hamiltonian structure and on Arnol'd's stability theorems. *J. Fluid. Mech.* **181**, 527–565.

Magnusdottir, G. & Haynes, P. H. 1999 Reflection of planetary waves in three-dimensional tropospheric flows. *J. Atmos. Sci.* **56**, 652–670.

Merkine, L.-O. 1977 Convective and absolute instabilities of baroclinic eddies. *Geophys. Astrophys. Fluid Dyn.* **9**, 129–157.

Merkine, L.-O. 1982 The stability of quasigeostrophic fields induced by potential vorticity sources. *J. Fluid Mech.* **116**, 315–342.

Nathan, T. R. 1997 Nonlinear spatial baroclinic instability in slowly varying zonal flow. *Dyn. Atmos. Oceans* **27**, 81–90.

Pedlosky, J. 1987 *Geophysical Fluid Dynamics*. Springer.

Pierrehumbert, R. T. 1983 Bounds on the growth of perturbations to non-parallel steady flow on the barotropic beta plane. *J. Atmos. Sci.* **40**, 1207–1217.

Pierrehumbert, R. T. 1984 Local and global baroclinic instability of zonally varying flow. *J. Atmos. Sci.* **41**, 2141–2162.

Pierrehumbert, R. T. 1986 Spatially amplifying modes of the Charney baroclinic-instability problem. *J. Fluid Mech.* **170**, 293–317.

Salmon, R. 1998 *Lectures on Geophysical Fluid Dynamics*. Oxford University Press.

Shepherd, T. G. 1990 Symmetries, conservation laws, and Hamiltonian structure in geophysical fluid dynamics. *Adv. Geophys.* **32**, 287–338.

Simmons, A. J., Wallace, J. M. & Branstator, G. W. 1983 Barotropic wave propagation and instability, and atmospheric teleconnection patterns. *J. Atmos. Sci.* **40**, 1363–1392.

Swanson, K. L. 2002 Dynamical aspects of extratropical troposphere low-frequency variability. *J. Climate* **15**, 2145–2162.